Reverse-time migration using the rapid expansion method (REM)

Alejandro Cabrales-Vargas

ABSTRACT

Reverse-time migration using the rapid expansion method allows the use of coarse time steps, and can be used as an alternative to high-order finite difference schemes. Its implementation using the pseudospectral method avoids the occurrence of frequency dispersion artifacts, and can be easily adapted to handling anisotropy. I use random boundary conditions to reduce memory usage.
Tests in two-dimensional synthetic models show the ability of this method to handle strong velocity and anisotropy contrasts in the presence of complex geology, regardless of the time resolution of the data.

INTRODUCTION

In recent years, reverse-time migration (RTM) has become a widely used imaging tool to produce high-quality images of the subsurface, primarily as a consequence of the petroleum exploration targeting ever more complex geological settings. Strong velocity contrasts, high-dip events, subsalt targets, and prismatic waves, among many other issues, constitute some of the challenges that seismic imagers have to deal with in their efforts to deliver the best possible subsurface images to seismic interpreters.

Although the first references about RTM can be traced back to the mid-70s, people usually refer to Baysal et al. (1983), Kosloff and Baysal (1983), Gazdag and Carrizo (1986), and McMechan (1983), among others, who set the basis for the post-stack RTM scenario. Meanwhile, Claerbout (1971) proposed the cross-correlation imaging condition to construct the subsurface image from downward- and upward-continued wavefields. This idea was later applied to forward and backward in time wavefield modeling, thereby constituting the basis for prestack RTM (Chang and McMechan, 1990; Loewenthal and Hu, 1991).

Solving the wave equation using implicit methods is prohibitive in practice for three-dimensional datasets (Claerbout, 1985). Therefore, geophysicists have opted for implementing explicit methods, accounting for keeping stability criteria, and avoiding frequency dispersion. One technique proposed to relax stability criteria and frequency dispersion restrictions is the rapid expansion method (REM) (Tal-Ezer et al., 1987; Etgen, 1989; Kosloff et al., 1989; Jastram and Behle, 1991; Stoffa and Pestana, 2009; Tessmer, 2011). This approximation is more accurate than the truncated Taylor series

based methods. It has been generally proposed in conjunction with a pseudospectral scheme, thus avoiding the problem of frequency dispersion. Nevertheless, it is worth mentioning that Jastram and Behle (1991) implemented the REM using staggered grids to solve elastic wave propagation.

Forward wavefield propagation generally consists of solving the two-way wave equation forward in time, and injecting a source signature at appropriate locations. Conversely, backward propagation consists of solving the same two-way wave equation, now backward in time, and injecting the receiver dataset of a single shot gather. The imaging condition is the zero-lag cross-correlation of such wavefields in the time domain for every shot profile. The final image is obtained by the superposition of the migrated shots. However, the cross-correlation imaging condition not only constructs reflection events related to the geology contrasts, but also low-frequency artifacts unique in RTM, caused by the cross-correlation of wavefronts propagating in the same direction in both wavefields. One solution proposed to tackle this problem is computing the Poynting vector (Yoon and Marfurt, 2006) to attenuate such artifacts by controling the angles of propagation of the wavefronts that are cross-correlated. Alternatively, Liu et al. (2011) proposed wavefield separation, recasting the imaging condition to perform the cross-correlation of wavefronts propagating in opposite directions exclusively. I implemented the latter solution to produce the RTM images for this report.

One problem associated with the cross-correlation of the source and the receiver wavefields is that every spatial frame (`x`,`z` plane in 2-D; `x`,`y`,`z` volume in 3-D) for all time steps has to be available, either loaded into memory (what easily overloads it), or stored on disk (which can make the I/O process rather slow). The reason is because the source and receiver wavefields are computed sequencially, forward and backward in time, respectively. Proposed solutions commonly involve checkpoint strategies (Symes, 2007). In this report l use random boundary conditions (RBC) (Clapp, 2009) to overcome this limitation, and compare the results to more conventional tapering boundary conditions (TBC) (Cerjan et al., 1985).

In the first part of this report, I present the formal derivation of the REM and the anisotropic solver (Zhan et al., 2012). Later, I present the application of the algorithm to 2D synthetic datasets: the Marmousi model with anisotropy (Alkhalifah, 1997), the Amoco 1997 2.5D model (Etgen and Regone, 1998; Dellinger et al., 2000), and the Hess VTI salt model. Then, I discuss the results and propose future steps. Finally, I present the conclusions of this report.

REVIEW OF THE RAPID EXPANSION METHOD THEORY

In this section I provide a review of the fundamentals of the REM.

Beginning with the 2D acoustic wave equation:

$$\frac{\partial^2 \mathbf{U}}{\partial t^2} = -\mathbf{L}^2\mathbf{U} + \mathbf{f}, \tag{1}$$

where $\mathbf{U}$ is the displacement field, $\mathbf{f}$ is the source term, the operator $-\mathbf{L}^2 = v(x,z)^2\nabla^2$ (the kernel), involving $v(x,z)$, which is the interval velocity, and the Laplacian operator

$$\nabla^2 = \frac{\partial^2}{\partial x^2} + \frac{\partial^2}{\partial z^2}. \tag{2}$$

$\mathbf{L}^2$ constitutes a matrix in the physical domain, and a scalar in the Fourier domain. I refer to Equation 1 as the inhomogeneous wave equation because, in general, the source term is not zero. When we explicitely set the source term equal to zero, Equation 1 becomes the homogeneous wave equation.

To perform RTM, we solve Equation 1 forward in time for the source wavefield, and backward in time for the receiver wavefield. Normally, source and receiver injection is employed to feed on the wavefields. However, using the REM we employ a different procedure to compute the source wavefield.

I find useful to set this problem from the point of view of linear algebra, because the set of solutions of the inhomogeneous wave equation constitutes a **linear variety**. It is represented as the superposition of the set of solutions for the homogeneous equation (the associated vector subspace), and one particular solution of the inhomogeneous equation (a known vector from the linear variety). The latter constitutes the period when the source is active, whereas the former constitutes the period after the source has shut down. This scheme is different to the source injection. On the other hand, the receiver wavefield backward propagation is conventionally solved with the homogeneous wave equation. There is no source in the sense of an independent term of the wave equation. Therefore, the receiver data are injected at every time step.

I elaborate more about these solutions in the following.

a) **Solution for the homogeneous equation**. This is the solution of Equation 1 without the source. We can propose a solution of the form (Stoffa and Pestana, 2009)

$$\mathbf{U}(t+\Delta t) = \mathbf{U}(t)\cos\mathbf{L}\Delta t + \frac{\partial \mathbf{U}(t)}{\partial t}\frac{\sin\mathbf{L}\Delta t}{\mathbf{L}}. \tag{3}$$

I dropped the spatial variables to simplify the notation. Now, we state the same solution backward in time:

$$\mathbf{U}(t-\Delta t) = \mathbf{U}(t)\cos\mathbf{L}\Delta t - \frac{\partial \mathbf{U}(t)}{\partial t}\frac{\sin\mathbf{L}\Delta t}{\mathbf{L}}. \tag{4}$$

and add it to Equation 3 to obtain:

$$\mathbf{U}(t+\Delta t)+\mathbf{U}(t-\Delta t)=2\mathbf{U}(t)\cos\mathbf{L}\Delta t. \tag{5}$$

Equation 5 is structured as a three-point stencil to be solved either forward or backward in time. We need an appropriate approximation for the cosine term to prevent the occurrence of frequency dispersion. Kosloff et al. (1989) modified the original algorithm proposed by Tal-Ezer et al. (1987), thereby expanding the cosine term to obtain:

$$\mathbf{U}(t+\Delta t)+\mathbf{U}(t-\Delta t)=\sum_{k=0}^{M/2}C_{2k}J_{2k}(\Delta tR)Q_{2k}\left(\frac{i\mathbf{L}}{R}\right)\mathbf{U}(t), \tag{6}$$

where $C_0=1$ and $C_k=2$ for $k>0$, J_k are the Bessel functions of first kind of order k, Q_k are modified Chebyshev polynomials of order k given by the following recursive expressions:

$$Q_0\left(\frac{i\mathbf{L}}{R}\right)=1, \tag{7}$$

$$Q_2\left(\frac{i\mathbf{L}}{R}\right)=1-\left(\frac{\mathbf{L}}{R}\right)^2, \tag{8}$$

$$Q_{k+2}\left(\frac{i\mathbf{L}}{R}\right)=\left[4\left(\frac{\mathbf{L}}{R}\right)^2+2\right]Q_k\left(\frac{i\mathbf{L}}{R}\right)-Q_{k-2}\left(\frac{i\mathbf{L}}{R}\right). \tag{9}$$

Finally, R is a constant that must be set larger than the largest eigenvalue of the operator $\mathbf{L}$ to ensure stability and convergence, and is given by:

$$R=v_{max}\pi\sqrt{\frac{1}{\Delta x^2}+\frac{1}{\Delta z^2}}. \tag{10}$$

Convergence is achieved by setting the number of terms of the series to $M>R\Delta t$.

As mentioned previously, Equation 6 can be solved both forward in time for the source wavefield and backward in time for the receiver wavefield, by isolating either $\mathbf{U}(t+\Delta t)$ or $\mathbf{U}(t-\Delta t)$, respectively. During the source wavefield modeling stage, we employ this solution for the period when the source is no longer active.

b) **Particular solution of the inhomogeneous equation**: This is the solution for the source wavefield propagation when the source term is active.

We first assume the source can be represented as:

$$\mathbf{f}(\mathbf{x},t)=\mathbf{g}(\mathbf{x})h(t), \tag{11}$$

where $\mathbf{g}(\mathbf{x})$ is the spatial position of the source, usually represented as an impulse function in $\mathbf{x}$, and $h(t)$ is the source signature. Under this assumption, the formal solution of Equation 1 is (Jastram and Behle, 1991)

$$\mathbf{U}(\mathbf{x},t) = \left[\int_0^t \frac{\sin(\tau\mathbf{L})}{\mathbf{L}} h(t-\tau)d\tau\right]\mathbf{g}(\mathbf{x}). \tag{12}$$

According to Stoffa and Pestana (2009), and Pestana and Stoffa (2010), we can approximate the solution as

$$\mathbf{U}(t,\mathbf{x}) = 2\sum_{k=1}^{M/2} b_{2k+1}(t)\frac{R}{i\mathbf{L}}Q_{2k+1}\left(\frac{i\mathbf{L}}{R}\right)\mathbf{g}(\mathbf{x}), \tag{13}$$

where

$$b_k(t) = \frac{1}{R}\int_0^t J_k(\tau R)h(t-\tau)d\tau. \tag{14}$$

The odd terms of the Chebyshev polynomials can be recursively obtained as (Chu and Stoffa, 2012):

$$\frac{R}{i\mathbf{L}}Q_1\left(\frac{i\mathbf{L}}{R}\right) = 1, \tag{15}$$

$$\frac{R}{i\mathbf{L}}Q_2\left(\frac{i\mathbf{L}}{R}\right) = 3 - 4\left(\frac{\mathbf{L}}{R}\right)^2, \tag{16}$$

$$\frac{R}{i\mathbf{L}}Q_{2k+1}\left(\frac{i\mathbf{L}}{R}\right) = 2\left[1 - 2\left(\frac{\mathbf{L}}{R}\right)^2\right]\frac{R}{i\mathbf{L}}Q_{2k-1}\left(\frac{i\mathbf{L}}{R}\right) - \frac{R}{i\mathbf{L}}Q_{2k-3}\left(\frac{i\mathbf{L}}{R}\right). \tag{17}$$

The factor $\frac{R}{i\mathbf{L}}$ is included to produce only real terms (even powers of $\frac{i\mathbf{L}}{R}$).

When the source shuts down, the source wavefield propagation continues with Equation 6.

Remember that the number of terms in the summations (Equations 6 and 13) depends on the product $R\Delta t$. R is a function of grid spacing. The finer the grid, the larger R becomes, and so does the number of terms in the series. Therefore, a finer grid demands more terms for the summations, more computational time to perform the Fourier transformations, and more memory usage. On the other hand, reducing the time sampling makes the number of terms in the series smaller, but increases the time steps, thereby demanding more computational resources too. There appears to be no point about coarsening or refining the time axis, at least with regards to run time, although the proof of this statement is beyond the scope of this report. For practical purposes I keep the original time sampling of the data in all the examples.

ANISOTROPY AND RAPID EXPANSION METHOD: DECOUPLED EQUATIONS FOT TILTED TRANSVERSE ISOTROPY

I implement the anisotropy with the pseudodifferential tilted transverse isotropy (TTI) decoupled equations proposed by Zhan et al. (2012), which are fully compatible with the REM, and prevents the appearance of residual SV-wave artifacts in the image. I do not derive here the TTI decoupled equations (the reader is referred to Zhan et al. (2012) for an excellent and concise derivation), but I merely replicate the terms for two dimensions, to illustrate their application in this report:

$$A_0 = k_x^2 + k_z^2 \tag{18}$$

$$A_1 = (2\epsilon \cos^4\theta + 2\delta \sin^2\theta \cos^2\theta))\frac{k_x^4}{k_x^2 + k_z^2} \tag{19}$$

$$A_2 = (2\epsilon \sin^4\theta + 2\delta \sin^2\theta \cos^2\theta))\frac{k_z^4}{k_x^2 + k_z^2} \tag{20}$$

$$A_3 = (-4\epsilon \sin 2\theta \cos^2\theta + \delta \sin 4\theta)\frac{k_x^3 k_z}{k_x^2 + k_z^2} \tag{21}$$

$$A_4 = (-4\epsilon \sin 2\theta \sin^2\theta - \delta \sin 4\theta)\frac{k_x k_z^3}{k_x^2 + k_z^2} \tag{22}$$

$$A_5 = (3\epsilon \sin^2 2\theta - 2\delta \sin^2 2\theta + 2\delta \cos^2 2\theta)\frac{k_x^2 k_z^2}{k_x^2 + k_z^2}. \tag{23}$$

In the last expressions, ϵ and δ correspond to the Thomsen's parameters (Thomsen, 1986), and θ constitutes the dip field. With these functions we can define a new kernel as

$$-\mathbf{L}^2 = -v(x,z)^2\big[A_0 + A_1 + A_2 + A_3 + A_4 + A_5\big]. \tag{24}$$

I note that, other than A_0 (which constitutes the isotropic term) we do not always need apply all terms. In case of vertical transverse isotropy (VTI) media, we can drop all the sine terms as $\theta = 0$, retaining only shorter versions of A_1 and A_5. Likewise, in the presence of eliptical anisotropy ($\epsilon \neq 0, \delta = 0, \theta = 0$) only A_1 is required.

METHODOLOGY AND IMPLEMENTATION

I implement RTM using the REM using the pseudospectral method, with the TTI decoupled equations when anisotropy is present. I compare images obtained applying TBC (Cerjan et al., 1985) to images obtained applying RBC (Clapp, 2009). I implement them by extending the image space 30 points each side, where such boundary conditions are applied. I attenuate the low-frequency artifacts by separating the wavefields according to Liu et al. (2011), thereby correlating wavefronts that propagate in opposite directions, corresponding to seismic reflections.

The most time-consuming process in REM-based RTM is the series summation. Computing and applying every term of the series is impractical and inefficient, because Chebyshev polynomials of different order share the same powers of the kernel, $-\mathbf{L}^2$. Every second power of the kernel signifies one sequence of 1) 2D/3D Fourier transform in space; 2) multiplication by the kernel; 3) 2D/3D inverse Fourier transform in space; and 4) multiplication by the velocity model. A much better approach is to group the precomputed coefficients of both the Chebyshev polynomials and the Bessel functions, so the computation of every second power of the kernel is performed only once.

RESULTS

In this section I present the results of applying REM-based RTM to synthetic models.

The first model is the Amoco 1997 2.5D dataset (Etgen and Regone, 1998; Dellinger et al., 2000), which is particularly challenging because of its high geological complexity and strong velocity variability (top of Figure 1), and at the same time suitable to test robust imaging techniques. The RTM results using TBC and RBC are shown at the center and the bottom of Figure 1, respectively.

The second model is the anisotropic Marmousi dataset (Alkhalifah, 1997) (left side of Figure 2). The right side of Figure 2 shows the η field that I used instead of the ϵ field, while both δ and θ fields are set to zero (Alkhalifah, email communication). The results are shown in Figure 3.

The third model is the Hess VTI salt model (second version of the dataset obtained using the SEPlib) (Figure 4). I decimated the dataset to a grid of 160 ft by 160 ft to speed up the calculations. The results are shown in Figure 5. I compensated the amplitudes by applying a linear depth gain.

DISCUSSION

In general, the results in the synthetic models demonstrate that the implementation of REM-based RTM be useful as an alternative to high-order finite differences approximation, without requiring any refinement of the recording time sampling.

In the Amoco 1997 2.5D dataset, the REM was capable of handling the strong lateral velocity contrasts by adequately defining the complexity of the salt layer, and preserving the steep faults above it, and properly imaging the flat detachment at the bottom of the section. It is worth noting that the time sampling is coarser than usual: 9.9 ms. Nevertheless, the results obtained showed that this issue was automatically accounted for by incorporating enough terms to the expansion series. On the other hand, the anisotropic version of the algorithm correctly images the Marmousi model with good quality in the definition of the faults, the shallow reflectors, and the geologic features at the reservoir level. Likewise, the same algorithm adequately positions the

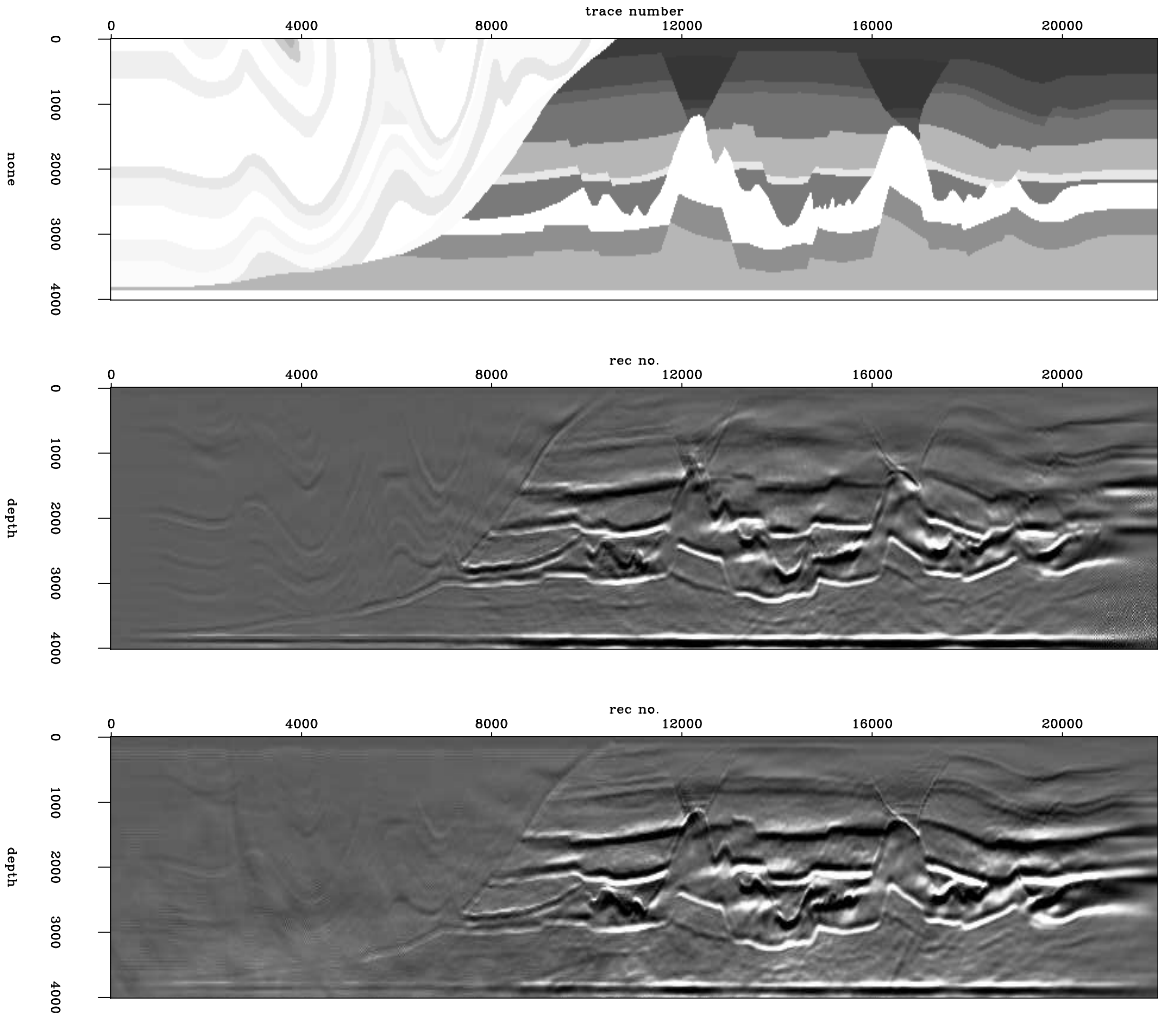

Figure 1: Amoco 1997 2.5D model. Top: Acoustic velocity field. Center: Reverse-time migration using tapering boundary conditions. Bottom: Reverse-time migration using random boundary conditions.

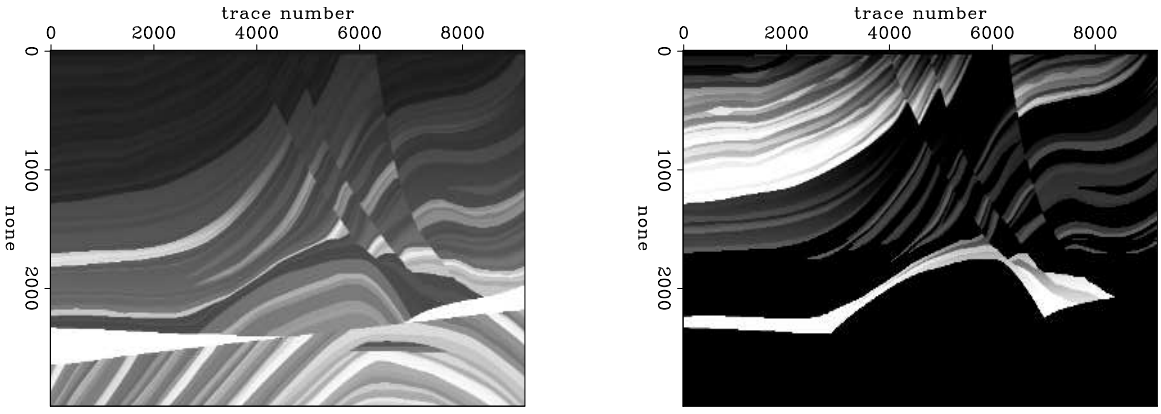

Figure 2: Anisotropic Marmousi model. Left: Acoustic velocity field. Right: η field.

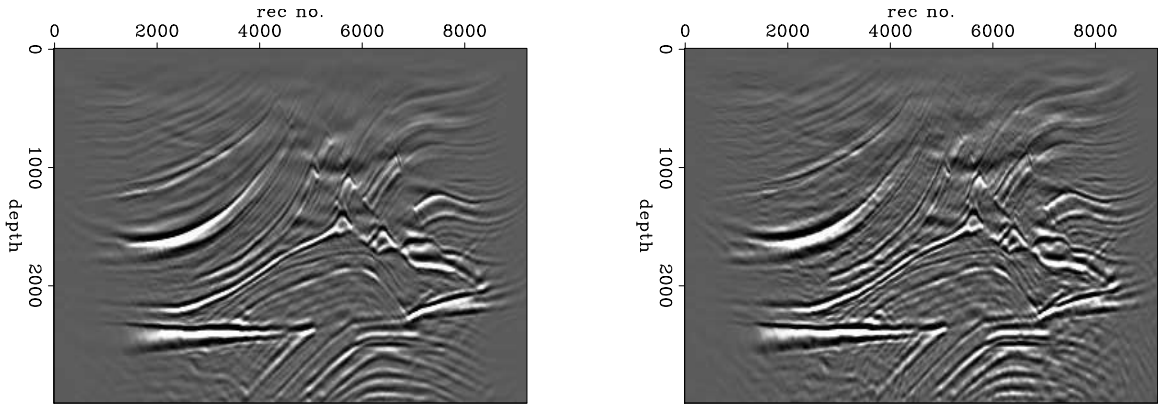

Figure 3: Reverse-time migration of the anisotropic Marmousi model. Left: Using tapering boundary conditions. Right: Using random boundary conditions.

salt body, the faults, and the reservoir reflections in the Hess VTI model. In all the migrated images there are still weak remnants of low-wavenumber artifacts.

Regarding the comparison between the boundary conditions, in the three datasets there is a tendency of the RBC to introduce both coherent and random noise, compared to the TBC. For instance, the Amoco 1997 2.5D RTM sections exhibit low-wavenumber noise and reverberating flat noise upon the the high-velocity hanging wall (on top of the thrust fault). The former appears to consist of remant low-wavenumber reflections that could not be "randomized" by the RBC. These different types of noise obscure this faint, low-amplitude part of the section (which has lower amplitude than the footwall in the original dataset). In contrast, the footwall exhibits some improvement details when using RBC: Layering around a 1 km depth is better defined, and there are sharper salt-sediment contrasts. Even part of the large-scale low-wavenumber shadow was attenuated in the footwall.

In the Marmousi RTM sections, we observe the inclusion of random noise when using RBC. There is neither apparent increase nor reduction of low-wavenumber artifacts.

Finally, in the Hess VTI RTM sections we observe aliasing artifacts related to spatial sampling decimation. Additionally, using RBC introduces random noise, particularly severe below the salt body, and above and below the reservoir levels. Interestingly, low-wavenumber noise observed when using TBC is absent using RBC.

CONCLUSIONS AND FUTURE WORK

- RTM implemented via REM produces images of good quality without the necessity of refining the recording time sampling. The best illustration of this fact is the migration of the Amoco 1997 2.5D dataset, that is sampled every 9.9 ms.
- TTI anisotropy can be properly handled by REM using the pseudospectral

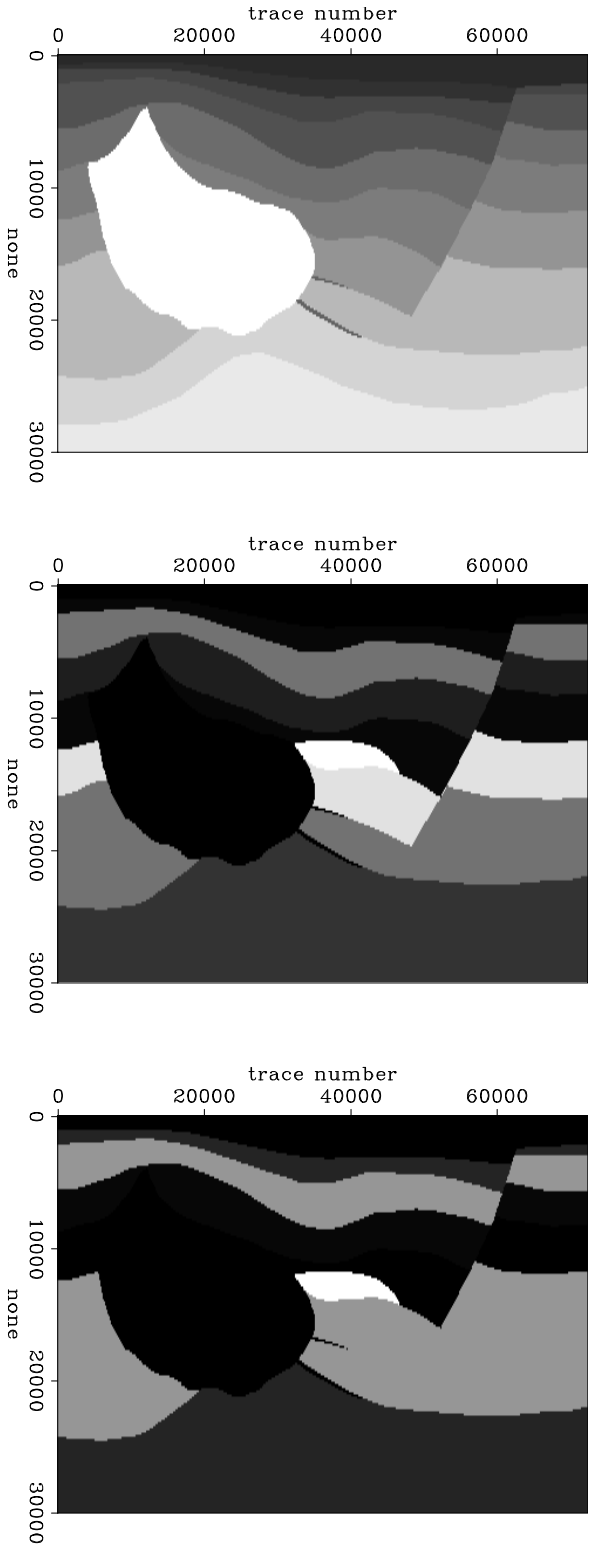

Figure 4: Hess VTI model. Top: Acoustic velocity field; center: ϵ field. Bottom: δ field.

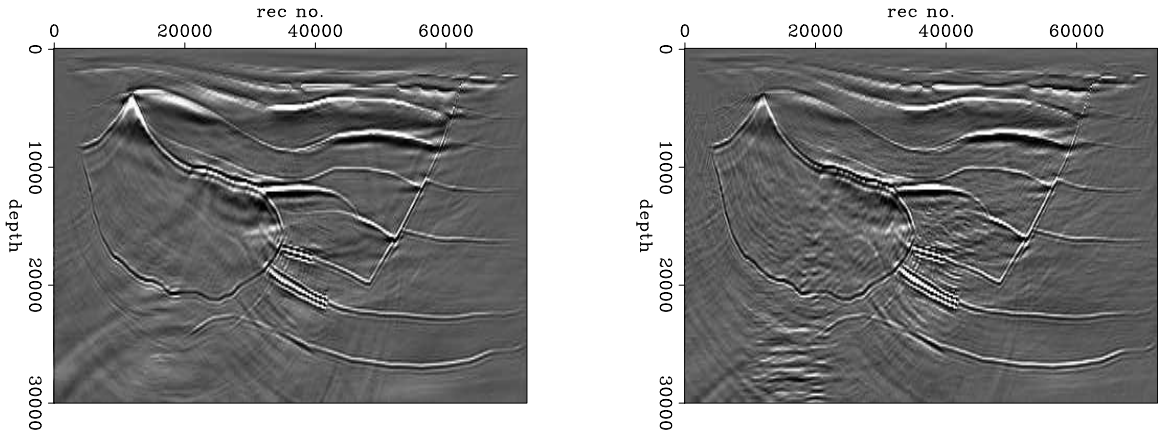

Figure 5: Reverse-time migration of the Hess VTI model. Left: Using tapering boundary conditions. Right: Using random boundary conditions.

approach, by means of the TTI decoupled equations.

- Using RBC highly reduces the memory usage, because only two spatial frames of every wavefield (corresponding to two time steps) are stored in memory.
- The comparisons between random boundaries reveals that in the current implementation there are still some artifacts related to the RBC, although some improvements in the sharpness of high-velocity contrasts (e.g., salt flanks) and better definition of reflections are observed in the Amoco 1997 2.5D RTM image, when using boundary conditions.
- Although RBC are very promising as an alternative to other optimization strategies to compute the imaging condition (e.g., checkpointing), in the current implementation care should be taken to minimize the artifacts.

Future actions include the following:

- Compare the REM performance to high-order finite differences
- Better suppression of the remaining low-frequency shadows in the final image
- Data-driven estimation of the source wavelet
- Computation of offset-domain and angle-domain common image gathers
- Exploration of more efficient anisotropy solvers
- Computation of the adjoint operator, for subsequent use in least-squares optimization

ACKNOWLEDGMENTS

I would like to thank Petroleos Mexicanos for the financial support, and Tariq Alkhalifah for the pertinent information about the usage of his Marmousi dataset. Very special thanks to Kurt Marfurt and the Attribute Assited Processing and Interpretation (AASPI) consortium, who allowed me to carry on the initial steps of this project using the University of Oklahoma servers. Last but not least, thanks to the SEP crew and sponsors.

REFERENCES

Alkhalifah, T., 1997, An acoustic wave equation for anisotropic media: SEP-Report, **95**, 283–307.

Baysal, E., D. Kosloff, and J. Sherwood, 1983, Reverse time migration: Geophysics, **48**, 1514–1524.

Cerjan, C., D. Kosloff, R. Kosloff, and M. Reshef, 1985, A nonreflecting boundary condition for discrete acoustic and elastic wave equations: Geophysics, **50**, 705–708.

Chang, W. and G. McMechan, 1990, 3D acoustic prestack reverse-time migration: Geophysical Prospecting, **38**, 737–755.

Chu, C. and P. Stoffa, 2012, Efficient 3D frequency response modeling with spectral accuracy by the rapid expansion method: Geophysics, **77**, no. 4, T117–T123.

Claerbout, J., 1971, Toward a unified theory of reflector mapping: Geophysics, **36**, 467–481.

Claerbout, J. F., 1985, Imaging the Earth's interior: Blackwell Scientific Publications, Inc.

Clapp, R. G., 2009, Reverse time migration with random boundaries: SEP-Report, **138**, 29–38.

Dellinger, J., S. Gray, G. Murphy, and J. Etgen, 2000, Efficient 2.5-D true-amplitude migration: Geophysics, **65**, 943–950.

Etgen, J., 1989, Accurate wave equation modeling: SEP-Report, **60**, 131–148.

Etgen, J. and C. Regone, 1998, Strike shooting, dip shooting, widepatch shooting - Does prestack depth migration care? A model study: SEG Technical Program Expanded Abstracts, 66–69.

Gazdag, J. and E. Carrizo, 1986, On reverse-time migration: Geophysical Prospecting, **34**, 822–832.

Jastram, C. and A. Behle, 1991, Elastic modeling by finite difference and the rapid expansion method (REM): SEG Technical Program Expanded Abstracts, 1573–1576.

Kosloff, D. and E. Baysal, 1983, Migration with the full acoustic wave equation: Geophysics, **48**, 677–687.

Kosloff, D., A. Filho, E. Tessmer, and A. Behle, 1989, Numerical solution of the acoustic and elastic wave equation by a new rapid expansion method: Geophysical Prospecting, **37**, 383–394.

Liu, F., Z. Guanquan, S. Morton, and J. Leveille, 2011, An effective imaging condition

for reverse-time migration using wavefield decomposition: Geophysics, **76**, no. 1, S29–S39.

Loewenthal, D. and L. Hu, 1991, Two methods for computing the imaging condition for common-shot prestack migration: Geophysics, **56**, 378–381.

McMechan, G., 1983, Migration by extrapolation of time-dependent boundary values: Geophysical Prospecting, **31**, 413–420.

Pestana, R. and P. Stoffa, 2010, Time evolution of the wave equation using rapid expansion method: Geophysics, **75**, no. 4, T121–T131.

Stoffa, P. and R. Pestana, 2009, Numerical solution of the acoustic wave equation by the rapid expansion method (REM) - A one step time evolution algorithm: SEG Technical Program Expanded Abstracts, 2672–2676.

Symes, W., 2007, Reverse time migration with optimal checkpointing: Geophysics, **72**, no. 5, SM213–SM221.

Tal-Ezer, H., D. Kosloff, and Z. Koren, 1987, An accurate scheme for seismic forward modelling: Geophysical Prospecting, **35**, 479–490.

Tessmer, E., 2011, Using the rapid expansion method for accurate time-stepping in modeling and reverse-time migration: Geophysics, **76**, no. 4, S177–S185.

Thomsen, L., 1986, Weak elastic anisotropy: Geophysics, **51**, 1954–1966.

Yoon, K. and K. Marfurt, 2006, Reverse-time migration using the Poynting vector: Exploration Geophysics, **37**, 102–107.

Zhan, G., R. Pestana, and P. Stoffa, 2012, Decoupled equations for reverse time migration in tilted transversely isotropic media: Geophysics, **77**, no. 2, T37–T45.